7516 *Biochemistry* **2010,** *49,* 7516–7523
DOI: 10.1021/bi1010128

BIOCHEMISTRY
including biophysical chemistry & molecular biology
Article

Infrared and EPR Spectroscopic Characterization of a Ni(I) Species Formed by Photolysis of a Catalytically Competent Ni(I)-CO Intermediate in the Acetyl-CoA Synthase Reaction[†]

Güneş Bender,[‡] Troy A. Stich,[§] Lifen Yan,[∥] R. David Britt,[§] Stephen P. Cramer,[∥,⊥] and Stephen W. Ragsdale*[,‡]

[‡]*Department of Biological Chemistry, University of Michigan, Ann Arbor, Michigan 48109,* [§]*Department of Chemistry, University of California, Davis, California 95616,* [∥]*Department of Applied Science, University of California, Davis, California 95616, and* [⊥]*Physical Biosciences Division, Lawrence Berkeley National Laboratory, Berkeley, California 94720*

Received June 23, 2010; Revised Manuscript Received July 28, 2010

ABSTRACT: Acetyl-CoA synthase (ACS) catalyzes the synthesis of acetyl-CoA from CO, coenzyme A (CoA), and a methyl group from the CH_3-Co^{3+} site in the corrinoid iron−sulfur protein (CFeSP). These are the key steps in the Wood−Ljungdahl pathway of anaerobic CO and CO_2 fixation. The active site of ACS is the A-cluster, which is an unusual nickel−iron−sulfur cluster. There is significant evidence for the catalytic intermediacy of a CO-bound paramagnetic Ni species, with an electronic configuration of $[Fe_4S_4]^{2+}$-(Ni_p^{+}-CO)-(Ni_d^{2+}), where Ni_p and Ni_d represent the Ni centers in the A-cluster that are proximal and distal to the $[Fe_4S_4]^{2+}$ cluster, respectively. This well-characterized Ni_p^{+}-CO intermediate is often called the NiFeC species. Photolysis of the Ni_p^{+}-CO state generates a novel Ni_p^{+} species (A_{red}*) with a rhombic electron paramagnetic resonance spectrum (*g* values of 2.56, 2.10, and 2.01) and an extremely low (1 kJ/mol) barrier for recombination with CO. We suggest that the photolytically generated A_{red}* species is (or is similar to) the Ni_p^{+} species that binds CO (to form the Ni_p^{+}-CO species) and the methyl group (to form Ni_p-CH_3) in the ACS catalytic mechanism. The results provide support for a binding site (an "alcove") for CO near Ni_p, indicated by X-ray crystallographic studies of the Xe-incubated enzyme. We propose that, during catalysis, a resting Ni_p^{2+} state predominates over the active Ni_p^{+} species (A_{red}*) that is trapped by the coupling of a one-electron transfer step to the binding of CO, which pulls the equilibrium toward Ni_p^{+}-CO formation.

Carbon monoxide dehydrogenase/acetyl-CoA synthase (CODH/ACS)[1] catalyzes the key steps in the Wood−Ljungdahl pathway of anaerobic CO_2 fixation, which provides carbon and energy for a variety of anaerobic microbes (*1*−*4*). This bifunctional enzyme consists of two central CODH subunits, each of which is attached to an ACS subunit, forming an $\alpha_2\beta_2$ complex (*5*, *6*). In the CODH subunit, CO_2 is reduced to CO, which then travels through a 70 Å tunnel to the A-cluster of ACS (*7*). Here, CO, a methyl group from the CH_3-Co^{3+} cofactor in the corrinoid iron−sulfur protein (CFeSP), and coenzyme A (CoA) (*1*) are converted to acetyl-CoA. On the basis of the results of X-ray crystallographic (*5*, *8*) and biochemical (*9*, *10*) studies, the active A-cluster is known to be composed of a $[Fe_4S_4]$ cluster bridged through cysteine to the proximal Ni (Ni_p) of a dinuclear Ni center (Figure 1), an arrangement similar to that for the Fe-only hydrogenases in which a $[Fe_4S_4]$ cluster and a binuclear Fe site are bridged by a Cys residue (*11*, *12*). The substrate binding site is ambiguous; however, computational results (*13*) combined with biochemical and spectroscopic experiments (*10*, *14*−*16*) and studies of model complexes (*17*, *18*) suggest that Ni_p is the binding site. Therefore, for the purpose of discussion, we will refer to the CO complex as involving Ni_p-CO, as shown in the mechanism in Figure 2. Ni_p changes ligation and oxidation states during catalysis, whereas the distal Ni (Ni_d), which is ligated by two deprotonated amides and two cysteine thiolates in a Cys-Gly-Cys motif, appears to remain square planar in the +2 oxidation state (*17*). Various details of the mechanism of acetyl-CoA synthesis have not yet been established; for example, whether Ni_p forms paramagnetic or diamagnetic intermediates during the reaction is debated (*1*, *19*−*21*). The paramagnetic mechanism, which is so-called because it includes a paramagnetic Ni(I)-CO species, is outlined in Figure 2. For the sake of simplicity, the ACS mechanism is described as an ordered reaction; however, recent isotope trapping experiments demonstrate that CO and the methyl group bind randomly to ACS, forming a ternary CH_3-Ni-CO (or binary acetyl) intermediate that reacts with CoA to form acetyl-CoA (*20*).

Because binding of CO is not a redox reaction, the Ni_p center in A_{red}* (prior to binding substrates, CO, or CH_3) should have the same redox state as Ni_p^{+}-CO, namely Ni_p^{+}, as shown in Figure 2. However, it is a conundrum that ACS lacks an electron paramagnetic resonance (EPR) signal before binding CO and becomes EPR-active afterward, because this would indicate that CO binding converts the enzyme from a diamagnetic to a paramagnetic state. Ironically, the best-characterized intermediate in

[†]This research was supported by grants to S.W.R. [National Institutes of Health (NIH) Grant GM-39451], S.P.C. (NIH Grant GM-65440, National Science Foundation Grant CHE-0745353, and DOE OBER), and R.D.B. (NIH Grant GM-48242).

*To whom correspondence should be addressed: Department of Biological Chemistry, University of Michigan Medical School, 1150 W. Medical Center Dr., Ann Arbor, MI 48109-0606. Telephone: (734) 615-4621. Fax: (734) 763-4581. E-mail: sragsdal@umich.edu.

[1]Abbreviations: CODH, CO dehydrogenase; ACS, acetyl-CoA synthase; FTIR, Fourier transform infrared; Ni_p, proximal nickel in the binuclear site of the A-cluster of ACS; Ni_d, distal nickel in the binuclear site of the A-cluster of ACS; DFT, density functional theory; EPR, electron paramagnetic resonance; A_{red}, state of the A-cluster in which ACS is treated with dithionite; A_{red}*, photolyzed state of A_{red}-CO; PDB, Protein Data Bank.

 Published on Web 07/29/2010

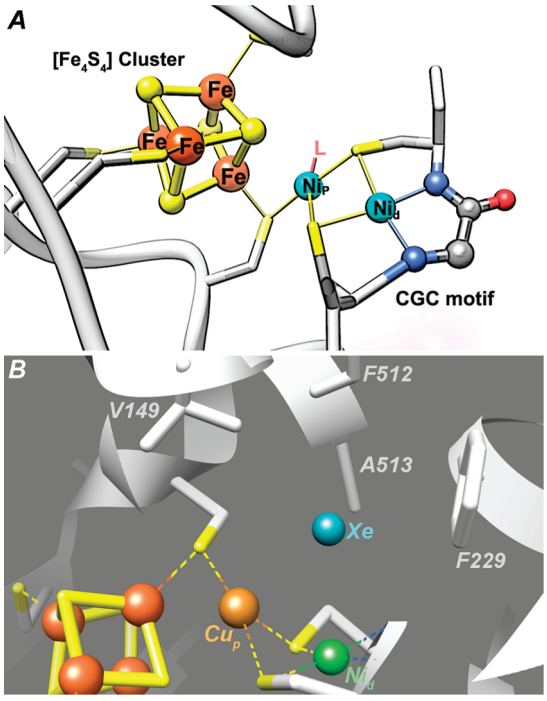

FIGURE 1: Structure of the A-cluster of ACS and the gas-binding site. (A) The structure is based on that of PDB entry 1OAO (*6*). (B) The structure is based on molecule P of PDB entry 2Z8Y (*7*), which was generated from a crystal structure obtained at high pressures of Xe. In this structure, Cu was present in the proximal site (Cu_p) and Ni was present in the distal site Ni_d. Some of the hydrophobic residues are shown that were proposed (*7*) to form a gas-binding site (the "alcove") near the binuclear center (Ni_p and Ni_d).

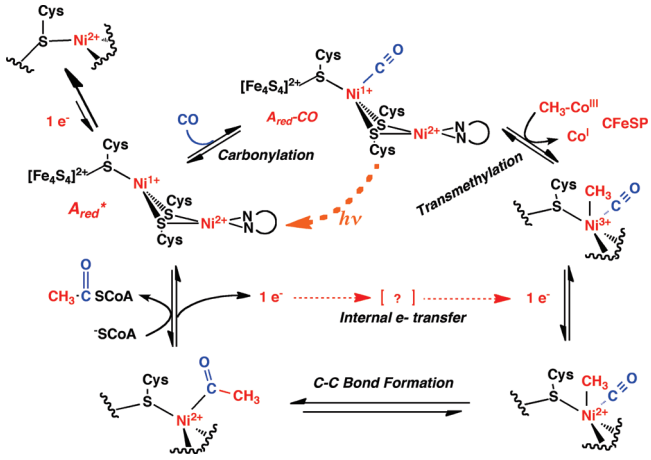

FIGURE 2: Paramagnetic mechanism of ACS. In this so-called "paramagnetic mechanism", which is written simplistically as an ordered reaction (although it is a random order of CO or methyl addition), CO traps the thermodynamically unfavorable Ni^+ state (A_{red}*). However, this state can be trapped at low temperatures by photolysis of the CO ligand. The A_{red}-CO state is favored because of CO backbonding to a low-valent Ni and because ACS has a CO binding site (alcove) near Ni_p. Transmethylation generates an unstable methyl-Ni^{3+} state that accepts an electron to generate the stable methyl-Ni^{2+} intermediate, which undergoes carbonyl insertion to generate an acetyl-Ni^{2+} intermediate. As the acetyl group undergoes thiolysis by the nucleophilic attack of CoA, two electrons bifurcate: one goes into the internal electron transfer pathway and the other is used to regenerate Ni^+. In the diamagnetic mechanism, so-called because none of the proposed intermediates are paramagnetic, the substrates bind to a diamagnetic "Ni(0)" state to generate a diamagnetic methyl-Ni(II) or Ni(II)-CO species. The intramolecular electron transfer step would not be required in the "diamagnetic mechanism". See the text for details.

the ACS mechanism is the most controversial one; this is the paramagnetic CO-bound Ni_p species (Ni_p^+-CO) (called A_{red}-CO or the "NiFeC species"), which has been trapped, spectroscopically characterized, and shown to be catalytically competent in acetyl-CoA synthesis (*22*). On the basis of density functional theory (DFT) computations that incorporate the results of EPR (*15*), Mössbauer (*23*, *24*), electron nuclear double resonance (ENDOR) (*25*), infrared (*26*, *27*), and X-ray crystallographic experiments (*11*, *12*), the electronic configuration of A_{red}-CO has been described as $[Fe_4S_4]^{2+}$-(Ni_p^+-CO)-(Ni_d^{2+}) (*13*). The assignment of this as a catalytically competent intermediate is based on its formation and decay rates being faster than the overall rate of acetyl-CoA formation (*22*, *27*, *28*). Furthermore, the results of combined freeze quench EPR and stopped-flow Fourier transform infrared (FTIR) experiments demonstrate that the NiFeC species is the sole metal-carbonyl species formed upon reaction of ACS with CO (*27*).

Besides Ni_p-CO, both methyl-ACS (*14*, *22*) and acetyl-ACS (*5*, *29*) species have been trapped, and these forms of the enzyme are EPR-silent and likely diamagnetic. The diamagnetic nature of methyl-ACS represents a challenge for the paramagnetic mechanism because rapid kinetic studies indicate that methyl transfer is an S_N2 reaction in which the methyl group is transferred formally as a cation; thus, nucleophilic attack of Ni_p^+ or Ni_p^+-CO on a methyl cation should generate a paramagnetic methyl-Ni^{3+} (or acetyl-Ni^{3+}) state. However, it is recognized that such a species would be highly oxidizing, possessing a $Ni^{3+/2+}$ couple perhaps as high as 1.0 V (*18*, *19*), and it has been proposed that a rapid coupled one-electron transfer could reduce the methyl-Ni^{3+} species to methyl-Ni^{2+} (*1*). Thus, the predominant observable species shown in Figure 2 that would accumulate to detectable levels during the catalytic mechanism would be Ni_p^{2+}, Ni^+-CO, methyl-Ni^{2+}, and acetyl-Ni^{2+}, while the unstable Ni_p^+ and methyl-Ni^{3+} states would be present in small amounts and observable only by special methods, like those described in this work.

Characterization of the photolysis of M-CO complexes, e.g., of the Fe^{2+}-CO state of heme in myoglobin or hemoglobin (*30*, *31*), has yielded important insights into protein structure, function, and dynamics. Detailed analysis of CO rebinding kinetics can provide information about different ligand binding sites and mechanisms (*32*). Here, we show that photolysis of the catalytically competent Ni_p^+-CO species at low temperatures generates a novel paramagnetic Ni_p^+ species with an extremely low barrier for recombination with CO. The photolysis and recombination have been characterized by EPR and IR measurements. The photolysis and spectroscopic studies described here provide significant novel insights into the mechanism of binding of CO to ACS and into the electronic structure of the A-cluster.

MATERIALS AND METHODS

Protein Purification. The His-tagged α-subunit (ACS) of the *Moorella thermoacetica* CODH/ACS was prepared, purified, and Ni-reconstituted under strictly anaerobic conditions with < 1 ppm of O_2 as described previously (*20*). For some ACS samples, Ni reconstitution was conducted for longer periods (2−3 days) and at a higher temperature (45 °C), which gave a higher NiFeC EPR spin quantity (60−75%).

FTIR Spectroscopy. The FTIR cell consisted of a 50 μm thick, airtight, transparent sample compartment and an outside metal frame. We prepared the samples used for FTIR by

incubating 100 μL of dithionite-reduced ACS (609 μM) with CO for 5 min, filling the FTIR cell in the anaerobic chamber using a blunt-ended syringe, removing the cell from the chamber, and freezing the sample immediately in liquid nitrogen. Then, the FTIR cell was transferred into a liquid helium cooling cryostat to start the experiment. Identical samples were prepared in H_2O and D_2O. Similar results were obtained with the H_2O- and D_2O-prepared samples; however, having D_2O as the solvent provided better access to the 1800−1600 cm^{-1} region of the spectrum, which includes the so-called "amide I region" where conformational changes in the polypeptide are observed.

EPR Spectroscopy. For the EPR-based detection of the photolysis reaction, we formed the Ni^+-CO intermediate by incubating 50−150 μM ACS with 2 mM dithionite and then purging the mixture with 100% CO for 15 min in an EPR tube. The spin concentration of the resultant A_{red}-CO, measured by double integration relative to a Cu perchlorate standard, was between 30 and 75% in different samples. Dithionite-reduced and methylated ACS samples were similarly prepared, but not treated with CO. Methylated ACS was prepared by incubation of 65 μM ACS with 2.5 equiv of methylcobinamide and 4 mM Ti(III) citrate at 45 °C for 2.5 h and removal of excess methylcobinamide by ultrafiltration. Acetylated ACS was prepared by purging the methylated ACS sample with 100% CO for 15 min in the EPR tube. X-Band (9.4 GHz) continuous-wave EPR spectra were recorded under nonsaturating, slow-passage conditions using a Bruker ECS106 spectrometer equipped with a TE_{102} cavity. Cryogenic temperatures were achieved and controlled using an Oxford Instruments ESR900 liquid helium cryostat in conjunction with an Oxford Instruments ITC503 temperature and gas flow controller.

Spectrometer settings for the data presented in Figure 6 included the following: temperature, 4.7 K; excitation frequency, 9.480 GHz; microwave power, 20 mW; modulation amplitude, 0.5 mT; modulation frequency, 100 kHz; sweep rate, 4.1 mT/s. The microwave power had to be reduced to 320 nW to give the NiFeC signal shown in the inset under nonsaturating conditions.

Photolysis and Recombination Experiments. For the FTIR experiments, sample photolysis was conducted in an Oxford cryostat with CaF_2 external windows, ZnSe intermediate windows, and ZnS windows for the IR cell. Spectra were recorded at 4 cm^{-1} resolution with a Bruker V-70 FT-IR spectrometer using an MCT detector. For photolysis, a 100 W XENOPHOT lamp (OSRAM HLX) source was located at the alternate source position of the Bruker spectrometer, and the sample was irradiated by turning the spectrometer mirrors to illuminate the sample with the alternative source. The estimated power on the sample was approximately 100 mW. The FTIR cell was irradiated at 4.7 K for different amounts of time as indicated in the legend of Figure 3. We observed the recombination after turning off the lamp, adjusting the temperature to one of the higher points indicated in Figure 4, and recording the kinetics at which the FTIR difference peak disappeared after the new temperature stabilized (within 90 s).

For the EPR experiments, photolysis was performed by focusing the IR-filtered [10 cm of an aqueous 10 mM $Cu(II)SO_4$ solution] light from a 300 W halogen incandescent lamp into the light port of the EPR cavity. The sample was rotated four times in 90° intervals each followed by continuous illumination for 15 min to maximize photolysis. No further intensity changes in the NiFeC signal were observed after illumination for this 1 h. The addition of 50% glycerol (v/v) to samples of A_{red}-CO led to a significant increase in the efficacy of the photolysis. Without glycerol, we observed an only 20% decrease in the magnitude of the NiFeC signal upon illumination. We attribute this change in yield to an increase in the optical quality of the frozen glass upon addition of glycerol. This has the effect of decreasing light scattering and allowing the incident light to penetrate more deeply into the 3 mm diameter EPR sample. For all reported data, a spectrum of the buffer collected under identical spectrometer conditions was subtracted. Data manipulations and spectral simulations were performed in MatLab using EasySpin 3.1 (*33*, *34*). Parameters used for the EPR spectral simulation presented in Figure 6 included the following: $S = {}^1/_2$, g = [2.56, 2.10, 2.01], g strain = [0.06, 0.015, 0.015], line width = 7 mT.

The recombination kinetics data obtained via FTIR spectroscopy were supported by analogous EPR experiments that

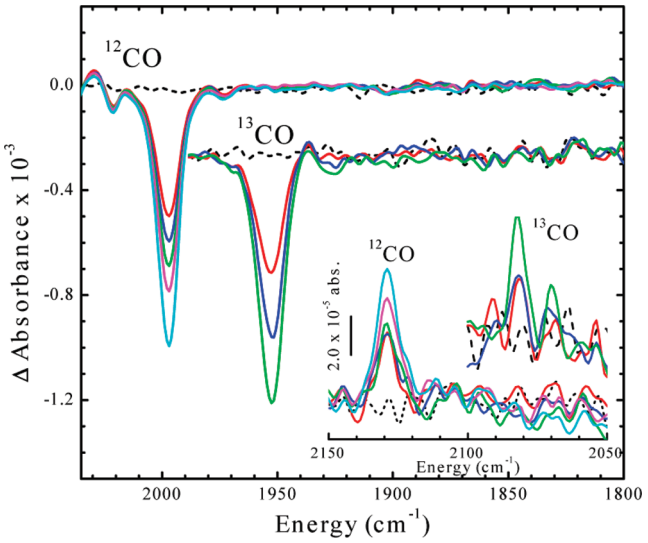

FIGURE 3: Time dependence of IR absorbance changes upon photolysis of A_{red}-CO at 4.5 K. The inset shows the development of features in the 2050−2150 cm^{-1} region, using ^{12}CO and ^{13}CO. See the Materials and Methods for details of the FTIR experiment. Time points for ^{12}CO data are 0 (black), 3 (red), 6 (blue), 12 (green), 20 (magenta), and 40 min (cyan). Time points for ^{13}CO data are 0 (black), 0.67 (red), 1.67 (blue), and 4 min (green). The ^{13}CO signal is enlarged 2.64-fold.

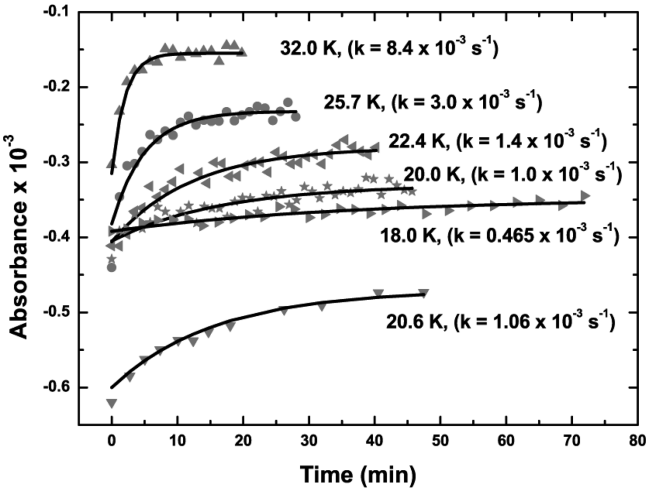

FIGURE 4: Time courses of thermal recombination at various temperatures. The temperatures at which the recombinations were observed and the fitted exponential rate constants are indicated next to the curves.

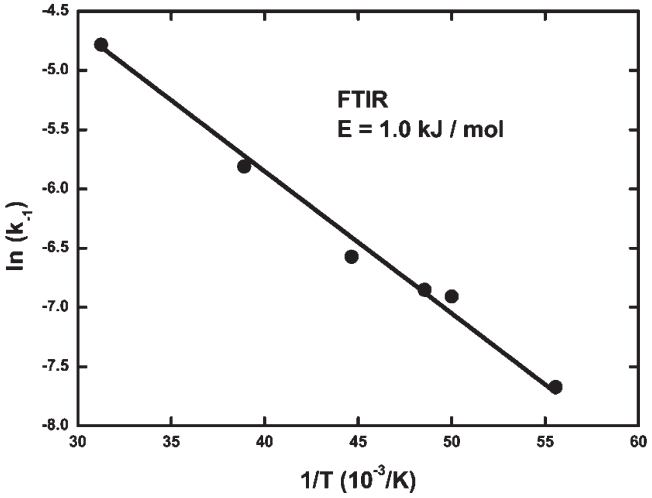

FIGURE 5: Arrhenius plot based on the data shown in Figure 4.

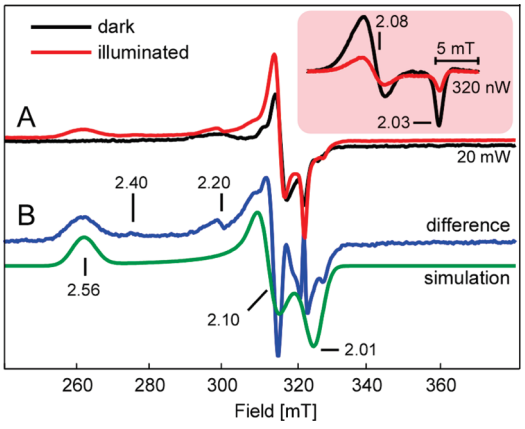

FIGURE 6: (A) X-Band EPR spectra (20 mW) of A_{red}-CO in 50% glycerol (v/v) (black) and A_{red}-CO after photolysis for 1 h at 4.7 K (red line). The inset shows the NiFeC signal measured using 320 nW of microwave power. (B) Difference of the two spectra in panel A (blue line) and corresponding simulation (green line). See the text for spectrometer settings and full simulation parameters.

monitored the recovery of the NiFeC signal, indicating successful recombination of CO and the transiently formed Ni^+ species, as a function of time once the lamp was extinguished. The sample was allowed to thermally equilibrate at 20.6 K for at least 15 min prior to the initiation of the experiment. This temperature was chosen for convenience and to allow for facile comparison of the kinetics measured via FTIR. The entire NiFeC signal was acquired in approximately 40 s. Successive scans were collected individually, and the intensity of the corresponding NiFeC signal was determined via double integration. With the onset of the illumination period of 8 min, the magnitude of the observed NiFeC signal diminishes significantly [10−12% (see Figure 8)]. Once the light is extinguished, we observed an immediate jump in the signal intensity followed by a much slower increase. It is likely that the first phase is due to sudden temperature changes in the sample caused by the cessation of illumination. Temperature stability returns rapidly, within one data point (i.e., 40 s). This second phase is well-fit by a signal-exponential function with a rate constant of ≈0.0006−0.0012 s^{-1}, in agreement with the 20.8 K recombination rate constant of 0.001 s^{-1} obtained from fitting the recovery of the ν(C≡O) band in the FTIR spectrum once the light is turned off (vide supra).

RESULTS

FTIR Studies of the Photolysis of A_{red}-CO and Recombination of CO with A_{red}.* Low-temperature (4.5 K) photolysis of A_{red}-CO generates a negative band at 1998 cm^{-1} in the difference FTIR spectrum (Figure 3). This is the first observation of any effect of photolysis on the FTIR (or EPR) spectra of A_{red}-CO. This feature shifts to a lower frequency (1953 cm^{-1}) when ACS is treated with ^{13}CO. This band and a similar isotope shift were first observed in FTIR studies of CO binding to CODH/ACS and assigned as a terminal carbonyl bound to the Ni center in ACS[2] (*26*). We attribute this loss of the ν(C≡O) stretching mode intensity to photoinduced breaking of the Ni−CO bond to generate CO and an A_{red}* species. Indeed, upon photolysis, a small positive band appears at 2129 cm^{-1} (2081 cm^{-1} when prepared with ^{13}CO) that is associated with unbound CO. When the temperature is increased, the negative CO bands disappear as the original Ni^+-CO species reappears (Figure 4); thus, photolysis must be conducted at low temperatures for A_{red}* to accumulate. Studies of the temperature dependence of the recombination rate reveal an exceptionally low activation energy (E_a) of 1 kJ/mol (Figure 5). For comparison, CO recombination to the Fe^{2+}-heme in myoglobin has an E_a of 8.4 kJ/mol (*35*).

EPR Studies of the Photolysis of A_{red}-CO and Recombination of CO with A_{red}.* The prephotolysis spectrum of A_{red}-CO (black trace, inset of Figure 6) is identical to that previously observed for the NiFeC signal (*15*). After continuous white-light illumination for 1 h at 4.7 K, the NiFeC signal intensity diminishes by 66% (red trace, inset of Figure 6) as a new set of resonances at ca. 260, 310, and 325 mT appear (Figure 6A). After subtraction of residual NiFeC contributions, the resultant A_{red}* signal is well-simulated as an $S = {}^1/_2$ spin system with g values of 2.56, 2.10, and 2.01 (Figure 6B). These signals are absent from the spectra of pre- or postphotolyzed ACS samples (A_{red}, A_{red}-CH_3, or A_{red}-$COCH_3$) lacking CO (Figure 7).

As in the FTIR experiment, photolysis of A_{red}-CO is only observed at low temperatures, and after photolysis, the NiFeC signal returns at a rate consistent with that measured by FTIR (cf. Figures 4 and 8). Thus, the formation of the paramagnetic photoproduct (A_{red}*) observed by EPR spectroscopy appears to be correlated with loss of the CO ligand in A_{red}-CO, observed by IR.

Other minor features at g values of 2.40 and 2.20 are observed in the difference EPR spectrum. These minor signals may arise from a slightly altered A_{red}* state, which is consistent with the appearance, in some samples of CO-treated ACS, of an altered form of the NiFeC signal with g values of 2.05 and 2.028 (*15*). It is also possible that these low-intensity resonances represent a small amount of Ni_d reduction; however, this is unlikely because spectroscopic and electrochemical studies of the $Ni^{2+/+}$ couple in model complexes with an N_2S_2 thiolato and carboxamido coordination environment reveal a very low midpoint potential (approximately −1.26 V vs the normal hydrogen electrode) that would not be accessible in aqueous solution with biological reductants (*18*, *36*). Thus, we suggest that the existence of these low-intensity features in the EPR spectra for the Ni_p center indicates variations in electronic and geometric environments, which has been observed after low-temperature photolysis of Mb-CO (*37*).

[2]In this citation, the M-CO band was assigned to CODH because it was not known until later (*64*) that CO oxidation and acetyl-CoA synthesis occur at separate sites.

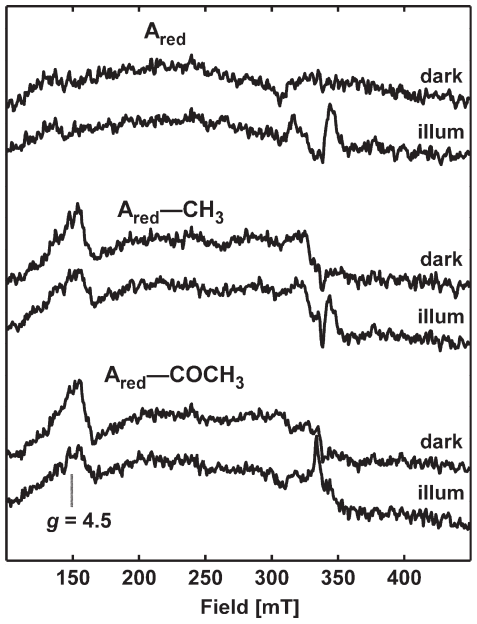

FIGURE 7: EPR spectra of A_{red} (top two spectra), A_{red}-CH_3 (middle), and A_{red}-$COCH_3$ (bottom) in 50% glycerol (v/v) before (dark) and after ("illum") white-light illumination for 1 h. In all cases, the spectrum of the buffer was subtracted. Spectrometer settings are identical to those used to acquire the data in Figure 6.

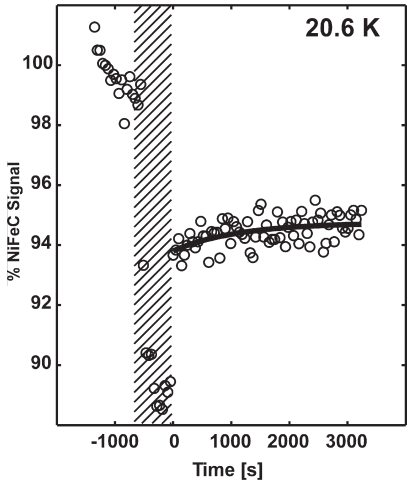

FIGURE 8: EPR spectral intensity of the NiFeC signal in A_{red}-CO with 50% glycerol (v/v) as a function of time and white-light illumination (designated by the hash marks). Spectrometer settings: temperature, 20.6 K; microwave frequency, 9.4744 GHz; microwave power, 6.41 μW; modulation frequency, 100 kHz; modulation amplitude, 0.5 mT; sweep rate, 0.73 mT/s.

DISCUSSION

This work describes photolysis studies of a catalytically competent metal-carbonyl species on ACS, the key enzyme in the Wood−Ljungdahl pathway of anaerobic CO_2 and CO fixation. Low-temperature (4.5 K) photolysis of the A_{red}-CO species generates a negative band at 1998 cm^{-1} in the difference FTIR spectrum (Figure 3). This feature shifts by 45 cm^{-1} to a lower frequency (1953 cm^{-1}) when ACS is incubated with ^{13}CO. This IR band has been previously observed in studies of CO binding to the *M. thermoacetica* CODH/ACS (*26*) and to the *Carboxydothermus hydrogenoformans* ACS (*27*) and was assigned to the stretching mode of a terminal carbonyl bound to the Ni center in ACS. The 1953 cm^{-1} IR band of A_{red}-^{13}CO exhibits an isotope shift when the ^{13}CO-incubated enzyme is reacted with natural abundance acetyl-CoA, indicating that the CO group of A_{red}-CO undergoes isotope exchange with the carbonyl group of acetyl-CoA (*26*). Furthermore, this IR band develops at catalytically relevant rates upon incubation of ACS with CO (*27*). These isotopic exchange experiments indicate that A_{red}-CO is a catalytically relevant intermediate in the mechanism of acetyl-CoA synthesis (*26*, *27*).

The IR band associated with A_{red}-CO forms at the same rate as an EPR signal with *g* values of 2.074 and 2.028 (*27*). This EPR signal has been called the NiFeC signal because it undergoes hyperfine-induced broadening when the metal centers in ACS are isotopically substituted with ^{61}Ni or ^{57}Fe and when ACS is incubated with ^{13}CO versus ^{12}CO (*15*). Here we describe EPR spectroscopic studies of the photolysis of A_{red}-CO. When we had earlier irradiated samples of CO-incubated CODH/ACS at 77 K in EPR tubes that were transferred into the EPR cavity for analysis, we did not observe any effects of photolysis on the NiFeC EPR signal (unpublished results). We now recognize that, as seen in the IR experiment, to observe photolysis, the experiment must be performed at low temperatures; for example, after continuous white-light illumination for 1 h at 4.7 K, the EPR signal intensity of A_{red}-CO is diminished by 66%.

These photolysis results have important implications for the structure of the CO binding site in ACS. We attribute the loss of the ν(C≡O) stretching mode intensity to photoinduced breaking of the Ni^{+}−CO bond to generate CO and a Ni^{1+} species (designated A_{red}*), a concept that is supported by the *g* values in the EPR experiments being similar to those of other Ni^{+} complexes (see below) and by the appearance of a small positive IR band (at 2129 cm^{-1} when ACS is reacted with ^{12}CO and 2081 cm^{-1} with ^{13}CO) that is associated with unbound CO. Such low temperatures are required to observe photolysis because recombination of CO with A_{red}* to generate the original Ni^{+}-CO species has an activation energy (E_a) of only 1 kJ/mol. The minimal E_a for recombination of CO with A_{red}* suggests that the nascent CO molecule cannot diffuse far from the Ni_p site. For comparison, CO recombination with the Fe^{2+}-heme in myoglobin has an E_a of 8.4 kJ/mol (*35*). FTIR (*38*, *39*) and X-ray crystallographic (*40*) studies of these heme-based systems indicate that, after photolysis, CO exits the active site and recombination kinetics depend on CO migration inside the protein as well as on protein dynamics accompanying the movement of CO. As shown in Figure 1B, a hydrophobic pocket located by crystallographic studies of Xe-incubated CODH/ACS is only 3.9 Å from Ni_p and has been proposed to represent the point of entry of CO into the A-cluster (*7*). Assuming a Ni_p−CO bond distance of 1.8 Å (*41*), CO would travel ≈2 Å to reach this hydrophobic binding pocket after the bond is broken. We propose that photolysis of A_{red}-CO could relocate CO into this alcove, a position from where it can rebind to Ni_p^{+} with a minimal E_a. The low E_a for CO recombination also implies that the photolysis and rebinding of CO at liquid He temperatures are not accompanied by any major reorganization of the active site conformation.

The photolysis results also have important implications with respect to the electronic and electrochemical properties of the A-cluster of ACS. Coupled to photoinduced loss of the Ni^{+}-CO species is the formation of a novel $S = {}^1/_2$ species with *g* values of 2.56, 2.10, and 2.01, which are appropriate for assignment of the

photolyzed state as a Ni(I) species (*42*−*44*). The unusually large *g* anisotropy found for A_{red}* indicates that the unpaired electron is almost wholly localized on Ni_p with very little spin density on the adjacent metal centers. Complexes that exhibit similar EPR spectra include a three-coordinate bisphosphine diethyl ether Ni complex (g = 2.45, 2.11, and 2.11) (*42*) and a tetrahedral tris-thioether Ni complex with bound CO (g = 2.64, 2.02, and 1.95) (*45*). The Ni-L form of [NiFe] hydrogenase (g = 2.3, 2.12, and 2.05), which is formed by photolysis of the H_2-reduced enzyme at 40 K (*46*), has much less *g* anisotropy because of the near square-pyramidal geometry of the Ni site and because exchange interactions with a neighboring Fe delocalize the electron density (*47*).

We do not observe any indication of the reduced [Fe_4-S_4] cluster (*g* values of 2.06, 1.92, and 1.80) (*48*) or of a Ti(III) citrate-reduced form of ACS that exhibits an axial EPR signal (g = 2.10 and 2.03) (*21*). There also is no evidence of the reduction of the Ni_d site. As described above, reduction of Ni_d would be highly unlikely on the basis of the very low midpoint potential of the $Ni^{2+/+}$ couple in model complexes with a similar coordination environment (*18*, *36*). Because an electron from the photolytically generated Ni_p^+ species could potentially transfer to either of the metal centers to which it is bridged, the predominance of the Ni_p^+ state suggests that, even though the redox potential for the $Ni^{2+/+}$ couple of Ni_p must be extremely low, those for the $[Fe_4S_4]^{2+/+}$ cluster and for $Ni_d{}^{2+/+}$ must be even lower (or their reductions are kinetically disfavored).

Importantly, the photolysis experiments allow the observation of a novel EPR active form of the A-cluster of ACS that is generated when CO is released; thus, this is the state that binds CO. As shown in Figure 2, we suggest that A_{red}* is a thermodynamically unfavorable Ni_p^+ state. The EPR signal of A_{red}* is not observed when ACS treated with reductants like Ti(III) citrate or dithionite because, in the absence of CO, the $Ni_p{}^{2+/+}$ equilibrium strongly favors Ni(II) (eq 1). In the presence of CO, the equilibrium shifts to favor the formation of Ni(I)-CO because CO tends to bind strongly to the low-valent states of metal centers [the K_m for CO in the CO/acetyl-CoA exchange is 10 μM (*49*)] and because there is a gas-binding pocket near Ni_p (*7*). Thus, it appears that, even in the presence of low-potential reductants with midpoint potentials below −500 mV, there is too little accumulation of the Ni_p^+ state for observation; however, by kinetically coupling the reduction (eq 1) and CO binding (eq 2) processes, formation of a low-valent Ni^+-CO complex becomes favorable. In a similar fashion, it was observed by cyclic voltammetry that the midpoint redox potentials of nickel(I) macrocyclic complexes shifted to a more positive value under 1 atm of CO (*50*).

$$\mathrm{Ni(II)} + \mathrm{e}^- \leftrightarrow \mathrm{Ni(I)} \quad (1)$$

$$\mathrm{Ni(I)} + \mathrm{CO} \leftrightarrow \mathrm{Ni(I)\text{-}CO} \quad (2)$$

Figure 2 shows two one-electron transfer steps that occur during the catalytic cycle. One is used to reductively activate Ni^{2+} to Ni^+ in the one-electron coupled CO binding step, and the other electron is used in the internal one-electron transfer associated with the methylation of ACS by the methylated CFeSP. These electrons ultimately come from CoA-dependent thiolysis of the acetyl-ACS intermediate to generate acetyl-CoA; thus, the overall reaction cycle does not involve net electron transfer. There is ample evidence of cryptic redox chemistry during acetyl-CoA synthesis; in fact, an unknown factor that was isolated on the basis of its ability to stimulate the CO/acetyl-CoA exchange reaction turned out to be ferredoxin, but it could be replaced by other mediators (*51*). Although CoA is the ultimate electron donor, the immediate donor(s) of the reducing equivalents involved in conversion of Ni^{2+} to Ni^+-CO and of methyl-Ni^{3+} to methyl-Ni^{2+} during the transmethylation reaction is unknown. Because the [Fe_4S_4] cluster that is attached to Ni_p is a low-potential center, we speculate that it could act as a conduit in the formation of A_{red}-CO. Although the transfer of electrons to and from the $[Fe_4S_4]^{2+/+}$ cluster has been shown to be 200-fold slower than the rate of methyl group transfer (*52*), coupling the electron transfer step to carbonylation in a so-called "EC reaction", i.e. electrochemical followed by chemical, would significantly enhance the rate because the thermodynamic driving force would be greater. We speculate that Ni_d may be involved in the redox-coupled methyl transfer reaction. Like other cobalamin-dependent transmethylations (*53*), this is a nucleophilic S_N2-type reaction (*54*, *55*) that would initially generate a methyl-Ni^{3+} intermediate; however, unlike methyl-Co^{3+}, methyl-Ni^{3+} is expected to be highly oxidizing and to undergo reduction to the methyl-Ni^{2+} state in the presence of even moderate reducing agents. The coordination environment of Ni_d resembles that of Ni-superoxide dismutase (Ni-SOD) (*56*, *57*), which accesses both the Ni^{2+} and Ni^{3+} states during the catalytic cycle (*56*, *58*). Furthermore, model studies have shown that Ni^{3+} is stabilized by the anionic amidate ligands found in Ni_d (*59*, *60*). Regardless, the paramagnetic pathway and the internal electron transfer loop in Figure 2 describe a speculative, but testable, working hypothesis that would include roles for all three components of the A-cluster.

In summary, we have demonstrated the photodissociation of CO from the Ni_p site in A_{red}-CO, which is a catalytically competent intermediate in acetyl-CoA synthesis (*22*, *27*, *28*). This is the first time a photolysis event has been observed on a catalytically competent metal-carbonyl intermediate on an enzyme. Though, CO photodissociation was observed in Ni-based inorganic compounds (*61*) and in Mo- and Ni-dependent nitrogenase and hydrogenase, respectively, for which CO acts as an inhibitor rather than a substrate (*62*, *63*). The other photoproduct (A_{red}*) is a Ni^+ species that is only long-lived at low temperatures ($t_{1/2}$ = 24.8 min at 18 K) and has EPR properties similar to those of Ni^+ compounds with trigonal planar or tetrahedral geometries. The facile recombination of CO with A_{red}* can be attributed to the capture of photolyzed CO in a gas-binding pocket near Ni_p that has been observed in the crystal structure (*7*). The $Ni_p{}^{2+/+}$ couple must have a sufficiently low redox potential that the Ni_p^+ photoproduct trapped in this study at low temperatures does not accumulate during catalysis. We propose that, during the ACS catalytic mechanism, binding of CO traps this unstable Ni_p^+ species in a coupled one-electron transfer step, pulling the redox equilibrium toward formation of Ni^+-CO. Further spectroscopic and computational studies of A_{red}* are underway and are expected to yield essential insight into changes in the electronic and geometric structures of the A-cluster that occur upon substrate binding.

ACKNOWLEDGMENT

We thank Elizabeth Pierce (University of Michigan) for help in preparing some of the enzyme used in these experiments.

REFERENCES

1. Ragsdale, S. W. (2004) Life with carbon monoxide. *Crit. Rev. Biochem. Mol. Biol. 39*, 165–195.
2. Ragsdale, S. W. (2007) Nickel and the Carbon Cycle. *J. Inorg. Biochem. 101*, 1657–1666.
3. Ragsdale, S. W. (2009) Nickel-based enzyme systems. *J. Biol. Chem. 284*, 18571–18575.
4. Müller, V., Imkamp, F., Rauwolf, A., Küsel, K., and Drake, H. L. (2004) Molecular and Cellular Biology of Acetogenic Bacteria. In Strict and Facultative Anaerobes: Medical and Environmental Aspects (Nakano, M. M., and Zuber, P., Eds.) pp 251−281, Horizon Bioscience, Wymondham, U.K.
5. Doukov, T. I., Iverson, T. M., Seravalli, J., Ragsdale, S. W., and Drennan, C. L. (2002) A Ni-Fe-Cu center in a bifunctional carbon monoxide dehydrogenase/acetyl-CoA synthase. *Science 298*, 567–572.
6. Darnault, C., Volbeda, A., Kim, E. J., Legrand, P., Vernede, X., Lindahl, P. A., and Fontecilla-Camps, J. C. (2003) Ni-Zn-[Fe_4-S_4] and Ni-Ni-[Fe_4-S_4] clusters in closed and open α subunits of acetyl-CoA synthase/carbon monoxide dehydrogenase. *Nat. Struct. Biol. 10*, 271–279.
7. Doukov, T. I., Blasiak, L. C., Seravalli, J., Ragsdale, S. W., and Drennan, C. L. (2008) Xenon in and at the end of the tunnel of bifunctional carbon monoxide dehydrogenase/acetyl-CoA synthase. *Biochemistry 47*, 3474–3483.
8. Drennan, C. L., Doukov, T. I., and Ragsdale, S. W. (2004) The metalloclusters of carbon monoxide dehydrogenase/acetyl-CoA synthase: A story in pictures. *J. Biol. Inorg. Chem. 9*, 511–515.
9. Seravalli, J., Xiao, Y. M., Gu, W. W., Cramer, S. P., Antholine, W. E., Krymov, V., Gerfen, G. J., and Ragsdale, S. W. (2004) Evidence that NiNi acetyl-CoA synthase is active and that the CuNi enzyme is not. *Biochemistry 43*, 3944–3955.
10. Seravalli, J., Xiao, Y., Gu, W., Cramer, S. P., Antholine, W. E., Krymov, V., Gerfen, G. J., and Ragsdale, S. W. (2004) Evidence That Ni-Ni Acetyl-CoA Synthase Is Active And That The Cu-Ni Enzyme Is Not. *Biochemistry 43*, 3944–3955.
11. Peters, J. W., Lanzilotta, W. N., Lemon, B. J., and Seefeldt, L. C. (1998) X-ray crystal structure of the Fe-only hydrogenase (Cpl) from *Clostridium pasteurianum* to 1.8 angstrom resolution. *Science 282*, 1853–1858.
12. Nicolet, Y., Lemon, B. J., Fontecilla-Camps, J. C., and Peters, J. W. (2000) A novel FeS cluster in Fe-only hydrogenases. *Trends Biochem. Sci. 25*, 138–143.
13. Schenker, R. P., and Brunold, T. C. (2003) Computational studies on the A cluster of acetyl-coenzyme A synthase: Geometric and electronic properties of the NiFeC species and mechanistic implications. *J. Am. Chem. Soc. 125*, 13962–13963.
14. Barondeau, D. P., and Lindahl, P. A. (1997) Methylation of carbon monoxide dehydrogenase from *Clostridium thermoaceticum* and mechanism of acetyl coenzyme A synthesis. *J. Am. Chem. Soc. 119*, 3959–3970.
15. Ragsdale, S. W., Wood, H. G., and Antholine, W. E. (1985) Evidence that an iron-nickel-carbon complex is formed by reaction of CO with the CO dehydrogenase from *Clostridium thermoaceticum*. *Proc. Natl. Acad. Sci. U.S.A. 82*, 6811–6814.
16. Bramlett, M. R., Tan, X., and Lindahl, P. A. (2003) Inactivation of Acetyl-CoA Synthase/Carbon Monoxide Dehydrogenase by Copper. *J. Am. Chem. Soc. 125*, 9316–9317.
17. Harrop, T. C., and Mascharak, P. K. (2005) Structural and spectroscopic models of the A-cluster of acetyl coenzyme a synthase/carbon monoxide dehydrogenase: Nature's Monsanto acetic acid catalyst. *Coord. Chem. Rev. 249*, 3007–3024.
18. Mathrubootham, V., Thomas, J., Staples, R., McCraken, J., Shearer, J., and Hegg, E. L. (2010) Bisamidate and Mixed Amine/Amidate NiN_2S_2 Complexes as Models for Nickel-Containing Acetyl Coenzyme A Synthase and Superoxide Dismutase: An Experimental and Computational Study. *Inorg. Chem. 49*, 5393–5406.
19. Hegg, E. L. (2004) Unraveling the structure and mechanism of acetyl-coenzyme A synthase. *Acc. Chem. Res. 37*, 775–783.
20. Seravalli, J., and Ragsdale, S. W. (2008) Pulse-chase studies of the synthesis of acetyl-CoA by carbon monoxide dehydrogenase/acetyl-CoA synthase: Evidence for a random mechanism of methyl and carbonyl addition. *J. Biol. Chem. 283*, 8384–8394.
21. Tan, X., Martinho, M., Stubna, A., Lindahl, P. A., and Munck, E. (2008) Mossbauer evidence for an exchange-coupled {$[Fe_4S_4]^{1+}$ Ni-p^{1+}} A-cluster in isolated α subunits of acetyl-coenzyme a synthase/carbon monoxide dehydrogenase. *J. Am. Chem. Soc. 130*, 6712–6713.
22. Seravalli, J., Kumar, M., and Ragsdale, S. W. (2002) Rapid kinetic studies of acetyl-CoA synthesis: Evidence supporting the catalytic intermediacy of a paramagnetic NiFeC species in the autotrophic Wood-Ljungdahl pathway. *Biochemistry 41*, 1807–1819.
23. Lindahl, P. A., Ragsdale, S. W., and Münck, E. (1990) Mössbauer studies of CO dehydrogenase from *Clostridium thermoaceticum*. *J. Biol. Chem. 265*, 3880–3888.
24. Xia, J., Hu, Z., Popescu, C. V., Lindahl, P. A., and Munck, E. (1997) Mössbauer and EPR Study of the Ni-Activated α-Subunit of Carbon Monoxide Dehydrogenase from *Clostridium thermoaceticum*. *J. Am. Chem. Soc. 119*, 8301–8312.
25. Fan, C., Gorst, C. M., Ragsdale, S. W., and Hoffman, B. M. (1991) Characterization of the Ni-Fe-C complex formed by reaction of carbon monoxide with the carbon monoxide dehydrogenase from *Clostridium thermoaceticum* by Q-band ENDOR. *Biochemistry 30*, 431–435.
26. Kumar, M., and Ragsdale, S. W. (1992) Characterization of the CO binding site of carbon monoxide dehydrogenase from *Clostridium thermoaceticum* by infrared spectroscopy. *J. Am. Chem. Soc. 114*, 8713–8715.
27. George, S. J., Seravalli, J., and Ragsdale, S. W. (2005) EPR and infrared spectroscopic evidence that a kinetically competent paramagnetic intermediate is formed when acetyl-coenzyme A synthase reacts with CO. *J. Am. Chem. Soc. 127*, 13500–13501.
28. Gorst, C. M., and Ragsdale, S. W. (1991) Characterization of a Ni-Fe-CO complex of CO dehydrogenase as a catalytically competent intermediate in the pathway of acetyl-CoA synthesis. *J. Biol. Chem. 266*, 20687–20693.
29. Gencic, S., and Grahame, D. A. (2008) Two Separate One-Electron Steps in the Reductive Activation of the A Cluster in Subunit β of the ACDS Complex in *Methanosarcina thermophila*. *Biochemistry 47*, 5544–5555.
30. Gibson, Q. H. (1956) An apparatus for flash photolysis and its application to the reactions of myoglobin with gases. *J. Physiol. 134*, 112–122.
31. Hartridge, H., and Roughton, F. J. W. (1923) The velocity with which carbon monoxide displaces oxygen from combination with haemoglobin. Part I. *Proc. R. Soc. London, Ser. B 94*, 336–367.
32. Abbruzzetti, S., Bruno, S., Faggiano, S., Ronda, L., Grandi, E., Mozzarelli, A., and Viappiani, C. (2008) Characterization of ligand migration mechanisms inside hemoglobins from the analysis of geminate rebinding kinetics. *Methods Enzymol. 437*, 329–345.
33. Stoll, S., and Britt, R. D. (2009) General and efficient simulation of pulse EPR spectra. *Phys. Chem. Chem. Phys. 11*, 6614–6625.
34. Stoll, S., and Schweiger, A. (2006) EasySpin, a comprehensive software package for spectral simulation and analysis in EPR. *J. Magn. Reson. 178*, 42–55.
35. Austin, R. H., Beeson, K. W., Eisenstein, L., Frauenfelder, H., and Gunsalus, I. C. (1975) Dynamics of ligand binding to myoglobin. *Biochemistry 14*, 5355–5373.
36. Hatlevik, O., Blanksma, M. C., Mathrubootham, V., Arif, A. M., and Hegg, E. L. (2004) Modeling carbon monoxide dehydrogenase/acetyl-CoA synthase (CODH/ACS): A trinuclear nickel complex employing deprotonated amides and bridging thiolates. *J. Biol. Inorg. Chem. 9*, 238–246.
37. Roder, H., Berendzen, J., Bowne, S. F., Frauenfelder, H., Sauke, T. B., Shyamsunder, E., and Weissman, M. B. (1984) Comparison of the magnetic properties of deoxy- and photodissociated myoglobin. *Proc. Natl. Acad. Sci. U.S.A. 81*, 2359–2363.
38. Causgrove, T. P., and Dyer, R. B. (1993) Protein Response to Photodissociation of CO from Carbonmonoxymyoglobin Probed by Time-Resolved Infrared-Spectroscopy of the Amide-I Band. *Biochemistry 32*, 11985–11991.
39. Plunkett, S. E., Chao, J. L., Tague, T. J., and Palmer, R. A. (1995) Time-Resolved Step-Scan FT-IR Spectroscopy of the Photodynamics of Carbonmonoxymyoglobin. *Appl. Spectrosc. 49*, 702–708.
40. Ostermann, A., Waschipky, R., Parak, F. G., and Nienhaus, G. U. (2000) Ligand binding and conformational motions in myoglobin. *Nature 404*, 205–208.
41. Furenlid, L. R., Renner, M. W., Szalda, D. J., and Fujiita, E. (1991) *J. Am. Chem. Soc. 113*, 883–892.
42. Saraev, V. V., Kraikivskii, P. B., Matveev, D. A., Zelinskii, S. N., and Lammertsma, K. (2006) EPR study of the oxidation reaction of nickel(0) phosphine complexes with Lewis and Bronsted acids. *Inorg. Chim. Acta 359*, 2314–2320.
43. Lancaster, J. R. (1988) The Bioinorganic Chemistry of Nickel, VCH, New York.
44. Albracht, S. P. J., Ankelfuchs, D., Bocher, R., Ellermann, J., Moll, J., Vanderzwaan, J. W., and Thauer, R. K. (1988) 5 New Electron-Paramagnetic-Res Signals Assigned to Nickel in Methyl-Coenzyme M-Reductase from *Methanobacterium thermoautotrophicum*, Strain Marburg. *Biochim. Biophys. Acta 955*, 86–102.

45. Craft, J. L., Mandimutsira, B. S., Flujita, K., Riordan, C. G., and Brunold, T. C. (2003) Spectroscopic and computational studies of a Ni^{+}-CO model complex: Implications for the acetyl-CoA synthase catalytic mechanism. *Inorg. Chem. 42*, 859–867.
46. Pandelia, M. E., Ogata, H., Currell, L. J., Flores, M., and Lubitz, W. (2010) Inhibition of the [NiFe] hydrogenase from Desulfovibrio vulgaris Miyazaki F by carbon monoxide: An FTIR and EPR spectroscopic study. *Biochim. Biophys. Acta 1797*, 304–313.
47. Ogata, H., Mizoguchi, Y., Mizuno, N., Miki, K., Adachi, S., Yasuoka, N., Yagi, T., Yamauchi, O., Hirota, S., and Higuchi, Y. (2002) Structural studies of the carbon monoxide complex of [NiFe]hydrogenase from *Desulfovibrio vulgaris* Miyazaki F: Suggestion for the initial activation site for dihydrogen. *J. Am. Chem. Soc. 124*, 11628–11635.
48. Bramlett, M. R., Stubna, A., Tan, X. S., Surovtsev, I. V., Munck, E., and Lindahl, P. A. (2006) Mossbauer and EPR study of recombinant acetyl-CoA synthase from *Moorella thermoacetica*. *Biochemistry 45*, 8674–8685.
49. Raybuck, S. A., Bastian, N. R., Orne-Johnson, W. H., and Walsh, C. T. (1988) Kinetic characterization of the carbon monoxide-acetyl-CoA (carbonyl group) exchange activity of the acetyl-CoA synthesizing CO dehydrogenase from *Clostridium thermoaceticum*. *Biochemistry 27*, 7698–7702.
50. Jung, H. J., Bang, H., and Suh, M. P. (2001) Carbon Monoxide Binding to Ni(I) Macrocyclic Complexes Generated by Electrochemical Methods. *Bull. Korean Chem. Soc. 22*, 523–525.
51. Ragsdale, S. W., and Wood, H. G. (1985) Acetate biosynthesis by acetogenic bacteria: Evidence that carbon monoxide dehydrogenase is the condensing enzyme that catalyzes the final steps of the synthesis. *J. Biol. Chem. 260*, 3970–3977.
52. Tan, X., Sewell, C., Yang, Q., and Lindahl, P. A. (2003) Reduction and Methyl Transfer Kinetics of the α Subunit from Acetyl Coenzyme A Synthase. *J. Am. Chem. Soc. 125*, 318–319.
53. Banerjee, R., and Ragsdale, S. W. (2003) The Many Faces of Vitamin B_{12}: Catalysis by Cobalamin-dependent Enzymes. *Annu. Rev. Biochem. 72*, 209–247.
54. Menon, S., and Ragsdale, S. W. (1998) Role of the [4Fe-4S] cluster in reductive activation of the cobalt center of the corrinoid iron-sulfur protein from *Clostridium thermoaceticum* during acetyl-CoA synthesis. *Biochemistry 37*, 5689–5698.
55. Menon, S., and Ragsdale, S. W. (1999) The role of an iron-sulfur cluster in an enzymatic methylation reaction: Methylation of CO dehydrogenase/acetyl-CoA synthase by the methylated corrinoid iron-sulfur protein. *J. Biol. Chem. 274*, 11513–11518.
56. Barondeau, D. P., Kassmann, C. J., Bruns, C. K., Tainer, J. A., and Getzoff, E. D. (2004) Nickel superoxide dismutase structure and mechanism. *Biochemistry 43*, 8038–8047.
57. Wuerges, J., Lee, J., Yim, Y., Kang, S., Yim, H., and Djinovic-Carugo, K. (2004) Crystal Structure of Nickel-Containing Superoxide Dismutase. *Proc. Natl. Acad. Sci. U.S.A. 101*, 8569–8574.
58. Bryngelson, P. A., and Maroney, M. J. (2007) Nickel superoxide dismutase. In Nickel and its Surprising Impact in Nature (Sigel, A., Sigel, H., and Sigel, R. K. O., Eds.) pp 417−444, John Wiley and Sons, West Sussex, England.
59. Mullins, C. S., Grapperhaus, C. A., and Kozlowski, P. M. (2006) Density functional theory investigations of NiN_2S_2 reactivity as a function of nitrogen donor type and N-H···S hydrogen bonding inspired by nickel-containing superoxide dismutase. *J. Biol. Inorg. Chem. 11*, 617–625.
60. Fiedler, A. T., Bryngelson, P. A., Maroney, M. J., and Brunold, T. C. (2005) Spectroscopic and computational studies of Ni superoxide dismutase: Electronic structure contributions to enzymatic function. *J. Am. Chem. Soc. 127*, 5449–5462.
61. Hennig, H., Hofbauer, K., Handke, K., and Stich, R. (1997) Unusual reaction pathways in the photolysis of diazido(phosphane)nickel(II) complexes: Nitrenes as intermediates in the formation of nickel(0) complexes. *Angew. Chem., Int. Ed. 36*, 408–410.
62. Vanderzwaan, J. W., Albracht, S. P. J., Fontijn, R. D., and Roelofs, Y. B. M. (1986) Electron-Paramagnetic-Res Evidence for Direct Interaction of Carbon-Monoxide with Nickel in Hydrogenase from *Chromatium vinosum*. *Biochim. Biophys. Acta 872*, 208–215.
63. Maskos, Z., and Hales, B. J. (2003) Photo-lability of CO bound to monitrogenase from *Azotobacter vinelandii*. *J. Inorg. Biochem. 93*, 11–17.
64. Kumar, M., Lu, W.-P., Liu, L., and Ragsdale, S. W. (1993) Kinetic evidence that carbon monoxide dehydrogenase catalyzes the oxidation of carbon monoxide and the synthesis of acetyl-CoA at separate metal clusters. *J. Am. Chem. Soc. 115*, 11646–11647.